Cancer Cell
Article

1B50-1, a mAb Raised against Recurrent Tumor Cells, Targets Liver Tumor-Initiating Cells by Binding to the Calcium Channel α2δ1 Subunit

Wei Zhao,[1,7] Limin Wang,[1,7] Haibo Han,[1] Kemin Jin,[2] Na Lin,[3] Ting Guo,[1] Yangde Chen,[4] Heping Cheng,[3] Fengmin Lu,[5] Weigang Fang,[6] Yu Wang,[1] Baocai Xing,[2,*] and Zhiqian Zhang[1,*]
[1]Key Laboratory of Carcinogenesis and Translational Research (Ministry of Education), Department of Cell Biology
[2]Department of Hepatobiliary Surgery I
Peking University Cancer Hospital and Institute, Beijing 100142, People's Republic of China
[3]State Key Laboratory of Biomembrane and Membrane Biotechnology, Institute of Molecular Medicine, Peking-Tsinghua Center for Life Sciences, Peking University, Beijing 100871, People's Republic of China
[4]Biologics Discovery, Genzyme, a Sanofi Company, Framingham, MA 01701, USA
[5]Department of Microbiology
[6]Department of Pathology
Peking University Health Science Center, Beijing 100191, People's Republic of China
[7]These authors contributed equally to this work
*Correspondence: xingbaocai88@sina.com (B.X.), zlzqzhang@bjmu.edu.cn (Z.Z.)
http://dx.doi.org/10.1016/j.ccr.2013.02.025

SUMMARY

The identification and targeted therapy of cells involved in hepatocellular carcinoma (HCC) recurrence remain challenging. Here, we generated a monoclonal antibody against recurrent HCC, 1B50-1, that bound the isoform 5 of the α2δ1 subunit of voltage-gated calcium channels and identified a subset of tumor-initiating cells (TICs) with stem cell-like properties. A surgical margin with cells detected by 1B50-1 predicted rapid recurrence. Furthermore, 1B50-1 had a therapeutic effect on HCC engraftments by eliminating TICs. Finally, α2δ1 knockdown reduced self-renewal and tumor formation capacities and induced apoptosis of TICs, whereas its overexpression led to enhanced sphere formation, which is regulated by calcium influx. Thus, α2δ1 is a functional liver TIC marker, and its inhibitors may serve as potential anti-HCC drugs.

INTRODUCTION

Hepatocellular carcinoma (HCC) is one of the deadliest cancers, mainly due to its high rate of recurrence, which can be as high as 70% following conventional treatments such as surgical resection, arterial embolization, and radiofrequency ablation (Llovet and Bruix, 2008; Xu et al., 2010). The cellular origin of HCC recurrence remains poorly understood, and, as yet, no specific treatment strategy has been developed that focuses on HCC recurrence.

HCC, like other cancer types, is composed of phenotypically and functionally diverse cell types (Shackleton et al., 2009; Visvader, 2011). It is hypothesized that a rare subset of cancer cells, often operationally referred to as cancer stem cells or tumor-initiating cells (TICs), behave like stem cells in that they are capable of self-renewal and of giving rise to a hierarchical organization of heterogeneous cancer cells. These cells are resistant to conventional chemotherapy and radiotherapy and, hence, are responsible for sustaining tumor growth and recurrence. Therapies that can eradicate these cells may eventually lead to cancer cures (Alison et al., 2011; Clarke et al., 2006; Rosen and Jordan, 2009; Visvader and Lindeman, 2012; Zhang et al., 2010). $CD133^+$, $CD13^+$, $CD24^+$, and $EpCAM^+$ cells, as well as some side populations from HCC cell lines and/or biopsies, have been identified as TICs, but their roles in HCC recurrence and therapeutic strategies to target these cells have only recently

Significance

This study identified a population of cells with the TIC properties and expressing α2δ1 in primary HCC and some surgical margins using the monoclonal antibody, 1B50-1. These TICs have prognostic value. α2δ1 was found to play an essential role in modulating calcium oscillation amplitude, which may be important in maintaining the properties of TICs. The study also suggested that α2δ1 could serve as a therapeutic target in the treatment of HCC. Additionally, 1B50-1 bound α2δ1 on TICs and could potentially be developed into an anti-HCC drug. These findings contribute to the understanding of HCC recurrence at both the cellular and molecular levels and advance the development of prognostic and therapeutic strategies.

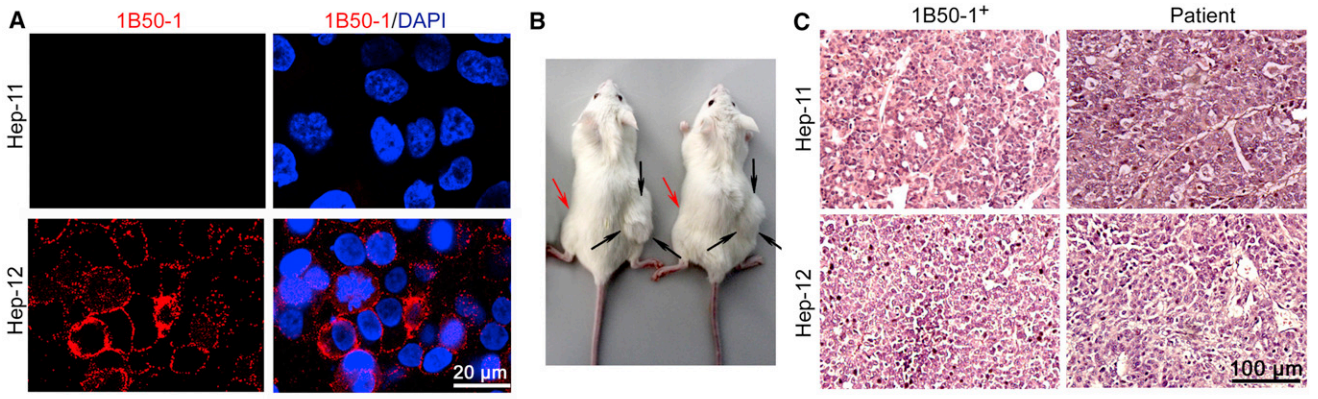

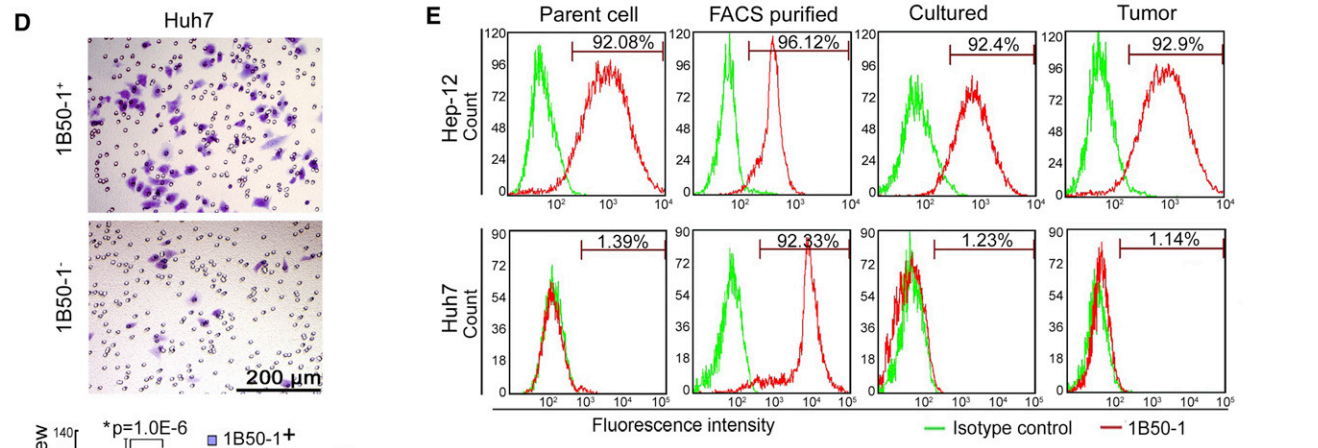

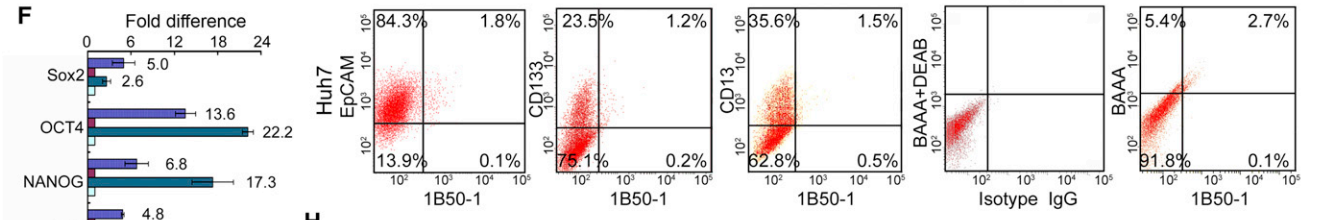

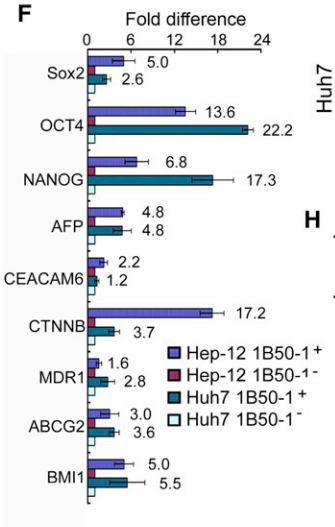

Web 3C

H

Markers	Tumor formation		Frequency of tumorigenic cells (95% CI)	p value
	10^3	10^2		
1B50-1$^+$CD133$^+$ (A)	5/5	5/5	1/1 (1/126-1/1)	4.67E-06 (A *vs* B)
1B50-1$^-$CD133$^+$ (B)	2/5	2/5	1/1061 (1/3129-1/360)	0.689 (B *vs* C)
1B50-1$^-$CD133$^-$ (C)	2/5	1/5	1/1445 (1/4728-1/442)	1.48E-06 (A *vs* C)
1B50-1$^+$CD13$^+$ (D)	5/5	4/5	1/62.6 (1/185-1/21.4)	2.28E-06 (D *vs* E)
1B50-1$^-$CD13$^+$ (E)	1/5	0/5	1/4983.8 (1/35192-1/706.2)	1.0 (E *vs* F)
1B50-1$^-$CD13$^-$ (F)	1/5	0/5	1/4983.8 (1/35192-1/706.2)	2.28E-06 (D *vs* F)
1B50-1$^+$EpCAM$^+$ (G)	5/5	5/5	1/1 (1/80.3-1/1)	8.5E-10 (G *vs* H)
1B50-1$^-$EpCAM$^+$ (H)	2/5	3/5	1/725 (1/1891.2-1/278)	0.11 (H *vs* I)
1B50-1$^-$EpCAM$^-$ (I)	1/5	1/5	1/2458 (1/10394.2-1/582)	8.9E-125 (G *vs* I)

(legend on next page)

begun to be investigated (Chiba et al., 2006; Haraguchi et al., 2010; Lee et al., 2011; Ma et al., 2010; Mishra et al., 2009; Yamashita et al., 2009).

Antibody-based targeted cancer therapy, either alone or in combination with standard chemotherapy regimens, has shown increasing clinical and commercial success (Deonarain et al., 2009). The current antibody-based anticancer therapies do not result in complete remission, but trials using antibodies targeting the surface molecules of TICs, such as DLL4, CD123, CD133, and interleukin-4 (IL-4), have shown promising therapeutic effects in a variety of cancers (Hoey et al., 2009; Jin et al., 2009; Rappa et al., 2008; Todaro et al., 2007). However, systematic identification of TIC biomarkers suitable for targeting antibody development is currently hindered by the sparseness of the TIC population in a given specimen.

We previously established a pair of HCC cell lines with the same clonal origin, Hep-11 and Hep-12, by primary culture from the same patient's primary and recurrent HCC tissues, respectively. Hep-12 cells are enriched for TICs, whereas Hep-11 cells do not form tumors in nonobese diabetic/severe combined immunodeficient (NOD/SCID) mice up to 6 months after injection of 5×10^6 cells (Xu et al., 2010). These two cell lines thus provide a unique cellular model system for characterizing the nature of the cells related to HCC recurrence and for identifying biomarkers for targeted therapy, specifically against recurrent HCC and perhaps for TICs in general. In this study, we used these two cell lines to generate monoclonal antibodies (mAbs) aiming to identify and target cells specifically related to HCC recurrence and to investigate the nature of these cells.

RESULTS

1B50-1 Identifies a Highly Tumorigenic and Invasive Subpopulation of HCC Cells

We used a whole-cell subtractive immunization approach (Brooks et al., 1993; Rasmussen and Ditzel, 2009) to generate mAbs that specifically reacted with Hep-12 cells. From three batches of cell fusions with the spleens of mice immunized with Hep-12 cells, a total of 37 hybridoma clones secreting mAbs that reacted strongly with Hep-12 cells, but weakly with Hep-11 cells, were obtained after screening with a cell-based ELISA method. One of these antibodies, named 1B50-1, recognized a subset of highly tumorigenic Hep-12 cells and appeared to be cytotoxic in vivo in our preliminary tumorigenicity assay. 1B50-1 bound to an antigen on the Hep-12 cell membrane, while it recognized few Hep-11 cells (Figure 1A). The percentage of cells bound by 1B50-1 (1B50-1$^+$) cells varied from 0.5% to less than 5% across HCC cell lines, with the exception of Hep-12 cells, more than 90% of which were 1B50-1$^+$ (Table 1).

To confirm that 1B50-1$^+$ cells have tumor initiation ability, we first purified 1B50-1$^+$ and 1B50-1$^-$ cells from five HCC cell lines by fluorescence-activated cell sorting (FACS) and performed tumorigenicity assays in NOD/SCID mice with limiting dilution. As shown in Table 1, as few as 100 purified 1B50-1$^+$ cells from the Huh7, Hep-12, HepG2, and SMMC7721 cell lines initiated tumor formation in almost all transplanted mice. For the least tumorigenic Hep-11 cell line, 1,000 purified 1B50-1$^+$ cells also resulted in tumor formation in five of five transplanted mice. The 1B50-1$^-$ counterparts either were completely nontumorigenic or formed tiny nodules only occasionally (Figure 1B; Figure S1A available online). We then tested the tumorigenic potential of 1B50-1$^+$ and 1B50-1$^-$ cells sorted from primary HCC-derived cells of four HCC patients. Again, 100 or 1,000 1B50-1$^+$ cells were consistently more tumorigenic than their 1B50-1$^-$ counterparts (Table 1; Figure S1A). Hematoxylin and eosin (H&E) staining demonstrated that the histological features of tumors formed by the 1B50-1$^+$ fractions resembled the tumors from which they derived, retaining the phenotypic heterogeneity, except those from Hep-12 cells, whose tumor morphology was slightly different from the original patient tissue (Figure 1C; Figure S1B).

We also compared the invasive property of 1B50-1$^+$ and 1B50-1$^-$ cells on Matrigel with a Boyden chamber assay. As shown in Figure 1D, 1B50-1$^+$ cells were more invasive than their 1B50-1$^-$ counterparts.

Differentiation Properties of 1B50-1$^+$ Cells

We next evaluated the differentiation potential of purified 1B50-1$^+$ cells from Hep-12 and Huh7 cell lines. After purified 1B50-1$^+$ Huh7 cells were cultured in vitro for 2 weeks, the percentage of 1B50-1$^+$ cells decreased from 92.33% to 1.23%, a value similar to that of the parental Huh7 population (Figure 1E). Furthermore, analysis of single-cell clones from Huh7 cells indicated that 1B50-1$^+$ cells underwent differentiation, giving rise to both 1B50-1$^+$ and 1B50-1$^-$ populations, whereas the percentage of 1B50-1$^+$ cells in the clones from the 1B50-1$^-$ fraction was unchanged (Figures S1C and S1D). It is important to note that the percentage of 1B50-1$^+$ cells in tumors formed by purified 1B50-1$^+$ Huh7 cells in NOD/SCID mice also decreased

Figure 1. Characterization of 1B50-1$^+$ HCC Cells

(A) Immunofluorescence staining for 1B50-1 in HCC cell lines. Nuclei were stained by DAPI.

(B) Representative photograph showing tumor formation in NOD/SCID mice injected s.c. with 1,000 sorted 1B50-1$^+$ (black arrows) and 1B50-1$^-$ (red arrows) Hep-11 cells.

(C) The histology of the tumors formed by 1B50-1$^+$ cells was compared with that of the HCC tissues from the original patient by H&E staining.

(D) Sorted 1B50-1$^+$ and 1B50-1$^-$ cells were assayed for their invasive ability on Matrigel using a Boyden chamber assay. Bars represent the mean ± SD of three independent experiments. *Student's t test.

(E) Flow cytometry results showing the percentage of 1B50-1$^+$ cells in parental cells, FACS-purified 1B50-1$^+$ cells and purified 1B50-1$^+$ cells cultured in 10% serum-containing medium for 2 weeks (Cultured) or transplanted into NOD/SCID mice (Tumor).

(F) qRT-PCR analysis of the expression of stem cell markers and drug-resistance-related genes in purified 1B50-1$^+$ and 1B50-1$^-$ populations. Data presented as fold difference over 1B50-1$^-$ cells for each gene, which was defined as 1 (calibrator). Error bars indicate SD.

(G) Representative flow cytometry results from analyzing indicated markers. For the ALDH assay, cells incubated with Aldefluor substrate BAAA and the ALDH-specific inhibitor DEAB were used to set the gate.

(H) Tumorigenic cell frequency in each fraction of Huh7 cells was determined with limiting dilution assay in NOD/SCID mice.

See also Figure S1.

Table 1. Tumorigenicity of 1B50-1$^+$ and 1B50-1$^-$ Cells Sorted from HCC Cell Lines and Clinical Specimen-Derived Cells in NOD/SCID Mice

	Percentage of Positive Cells				Positive in 1B50-1$^+$ Cells (%)			Tumor Formation (Tumor Formed/Mice Injected)			
								1B50-1 Positive		1B50-1 Negative	
Cells	1B50-1[a]	CD133	CD13	EpCAM	CD133	CD13	EpCAM	10^3	10^2	10^3	10^2
Huh7	0.9–2.2	24.7	37.1	86.1	85.7	75	94.7	5/5(3.8 ± 1.9)[b]	5/5	3/5(0.09 ± 0.06)[b]	0/5
Hep-11	0.4–0.7	91.2	97.4	99.9	100	100	97.8	5/5	1/5	0/5	0/5
Hep-12	92.1–94.8	76.3	97.1	99.7	78.5	98.4	99.9	5/5(4.5 ± 1.1)[b]	5/5	3/5(1.3 ± 0.3)[b]	0/5
HepG2	0.5–2.1	4.2	53.4	4.8	85.5	94.3	85.7	4/5	4/5	0/5	0/5
SMMC7721	0.5–0.6	4.8	23.2	3.6	94.3	86	85.1	5/5	5/5	0/5	0/5
Case-1[c]	1.7–3.3	2.4	30.3	28.8	84.3	92.1	97.6	5/5(3.5 ± 1.0)[b]	5/5	3/5(0.12 ± 0.04)[b]	0/5
Case-2[c]	0.6–2.1	2.1	87.7	2.5	90.3	97.6	78.7	3/5	2/5	0/5	0/5
Case-3[c]	0.4–1.8	1.5	85.5	15.8	96.8	91.7	95.2	5/5(1.3 ± 0.6)[b]	3/5	5/5(0.6 ± 0.4)[b]	1/5
Case-4[c]	0.6–1.3	8.6	13.7	4.1	89.8	93.7	91.8	2/5	0/5	0/5	0/5

[a]The results of two to eight flow cytometry analyses.
[b]The data in the parentheses are the average volume ± SD of tumors formed (cm^3).
[c]HCC specimens were undergone primary culture and expanded in vitro for less than ten passages.

to 1.14% (Figure 1E). These data suggest that 1B50-1$^+$ cells are able to differentiate into 1B50-1$^-$ cells but not vice versa. However, purified 1B50-1$^+$ Hep-12 cells retained their high percentage of 1B50-1$^+$ cells whether they were kept in culture or in vivo, like the parental Hep-12 cells (Figure 1E; Figure S1E).

1B50-1$^+$ Cells Express Multiple Stem Cell Genes

To confirm that 1B50-1$^+$ cells represent cells with stem cell-like properties at the molecular level, the expression of a panel of genes associated with liver progenitor cells (Sell and Leffert, 2008) was compared between 1B50-1$^+$ and 1B50-1$^-$ populations purified from Hep-12 and Huh7 cells by quantitative reverse transcription (qRT)-PCR (Figure 1F). Compared with 1B50-1$^-$ cells, 1B50-1$^+$ cells from both cell lines consistently expressed higher levels of *OCT4*, *SOX2*, *NANOG*, *BMI1*, *AFP*, and *CTNNB*. Furthermore, the expression of the drug efflux transporter gene *ABCG2* and the multidrug resistance gene *MDR1* was elevated in the 1B50-1$^+$ fractions.

It is interesting that 1B50-1$^+$ cells overlapped with CD133$^+$, EpCAM$^+$, CD13$^+$, and ALDH$^+$ populations of Hep-12 cells (Figure 1G). Although the majority of 1B50-1$^+$ cells were also positive for CD133, EpCAM, CD13, and ALDH in Huh7 cells, only a small fraction of CD133$^+$, EpCAM$^+$, CD13$^+$, or ALDH$^+$ cells were 1B50-1$^+$ (Figure 1G). A similar correlation between 1B50-1 and these reported HCC TIC markers was also found in other HCC cell lines and patient-derived cells (Table 1). Thus, 1B50-1$^+$ cells represent fractions of CD133$^+$, EpCAM$^+$, and CD13$^+$ populations but not vice versa.

1B50-1$^+$ Cells Are a More Restricted Subset of Highly Tumorigenic Cells among CD13$^+$, CD133$^+$, and EpCAM$^+$ HCC TIC Populations

The relationship of 1B50-1 to the other liver TIC markers CD13, CD133, and EpCAM and the fact that the 1B50-1$^+$ fraction of nontumorigenic Hep-11 cells, which were more than 91% positive for CD13, CD133, and EpCAM, was tumorigenic led us to propose that the previously reported HCC TIC population defined by CD13$^+$, CD133$^+$, or EpCAM$^+$ might be mainly attributed to the existence of their respective 1B50-1$^+$ subsets. To confirm this, we compared the tumor-forming ability of different fractions of Huh7 cells (Figure 1H). As few as 100 cells of 1B50-1$^+$CD13$^+$, 1B50-1$^+$CD133$^+$, and 1B50-1$^+$EpCAM$^+$ subsets formed tumors in almost all the transplanted mice, whereas only small nodules were occasionally found in all other fractions that were 1B50-1$^-$. Cells only positive for CD13, CD133, or EpCAM did not have significantly higher tumor formation ability compared with each corresponding double-negative fraction.

Clinical Significance of 1B50-1$^+$ Cells in HCC and Surgical Margin Tissues

Because 1B50-1 did not stain formalin-fixed tissues, we examined its staining by fluorescence immunohistochemistry using 86 paired frozen HCC and paracancerous tissues that were obtained from the hepatectomy margins, six recurrent HCC tissues, and five normal liver samples from hepatic hemangioma patients. As shown in Figure 2A, 1B50-1 reacted with an antigen on the cell surface in the positive tissues and 1B50-1$^+$ cells showed a scattered distribution in 72.1% of HCC tissues, whereas they were detected in only 46.5% of paracancerous tissues (Table S1). Furthermore, 1B50-1$^+$ staining in paracancerous tissues was only found in those patients with positive staining in their tumor tissues. No 1B50-1$^+$ cells were observed in the five normal liver tissues. It is important to note that 1B50-1$^+$ cells were enriched in the recurrent HCC tissues of four patients out of six tested.

Next, we examined the tumorigenic capability of 1B50-1$^+$ and 1B50-1$^-$ cells sorted directly from freshly resected HCC and paracancerous tissues of three patients (Figure 2B). 1B50-1$^+$ cells isolated from the tumor tissues of all three patients gave rise to tumor growth after transplantation of as few as 1,000 cells, while those purified from the paracancerous tissues in two out of three patients also initiated tumor growth within 8 weeks after transplantation. As many as 10^5 1B50-1$^-$ cells isolated from either tumor or paracancerous tissues caused no visible tumor formation after 4 months. H&E staining showed no difference in the

histology formed by 1B50-1$^+$ cells from tumor versus peritumor tissues, which both resembled that of the tumor tissue of the patient (Figure 2C).

Finally, we analyzed the correlation between the clinicopathologic characteristics and 1B50-1 staining status (Table S1). No significant correlation was found between the 1B50-1$^+$ staining in HCC tissues and any clinicopathologic factor. However, the presence of 1B50-1$^+$ cells in the paracancerous tissues did correlate significantly with hepatic cirrhosis, very rapid recurrence, and a lower rate of 4-year overall survival postsurgery. Kaplan-Meier curves revealed that the 1B50-1 staining status in the tumor tissues did not correlate with disease-free or overall survival of these patients, but the median disease-free survival and the 75th percentile overall survival time postsurgery in the patients with 1B50-1$^-$ staining in the paracancerous tissues were approximately 4.5 and 10.1 times, respectively, those with positive staining (Figures 2D–2G). Multivariant Cox regression analysis also showed that 1B50-1$^+$ staining in HCC paracancerous tissues was an independent risk factor of poor prognosis for HCC patients (Figure 2H).

Self-Renewal Property of 1B50-1$^+$ Cells

To further confirm that 1B50-1$^+$ cells have stem cell-like properties, we first performed sphere formation assays to determine their in vitro self-renewal ability. 1B50-1$^+$ cells purified from various HCC cell lines and clinical specimens displayed significantly higher sphere-forming efficiency compared with their respective 1B50-1$^-$ counterparts. Furthermore, the sphere-forming ability of 1B50-1$^+$ cells expanded in subsequent serial propagations (Figures 3A and 3B). We then performed in vivo serial transplantation assays with resorted cells from tumors formed by 1B50-1$^+$ cells. Once again, 1B50-1$^+$ cells formed tumors in the second transplanted mice, while their 1B50-1$^-$ counterparts remained nontumorigenic (Figure 3C). These results demonstrate that 1B50-1$^+$ cells have self-renewal ability both in vitro and in vivo.

In Vitro Effects of 1B50-1 on HCC Cells

To evaluate if 1B50-1 could have some effects on liver TICs, we first tested the sphere-forming ability of 1B50-1$^+$ cells following 1B50-1 treatment. As shown in Figure 3D, 1B50-1 at 10 μg/ml significantly suppressed the sphere formation of 1B50-1$^+$ cells purified from all HCC cell lines and patient-derived specimens tested.

We then examined the effect of 1B50-1 on the apoptosis of 1B50-1$^+$ cells by a terminal deoxynucleotidyl transferase dUTP nick-end labeling (TUNEL) assay. 1B50-1 induced apoptosis of the cultured Hep-12 cells in a dose-dependent manner. The apoptosis-inducing effect was also confirmed in 1B50-1$^+$ fractions purified from other cell lines. No significant cell apoptosis was observed for unpurified Hep-11 cells upon 1B50-1 treatment (Figures 3E and 3F; Figure S2).

Finally, we treated cultured HCC cells with 1B50-1 at 10 μg/ml for 48 hr, followed by transplanting the cells into NOD/SCID mice subcutaneously (s.c.) with limiting dilution. While 10^6 cells of control groups (treated with immunoglobulin G [IgG]) formed tumors in all the transplanted mice within 3–4 weeks after injection, none of the mice transplanted with 1B50-1-treated cells showed tumor formation after 12 weeks (Figure 3G). These data indicate that tumorigenic cells are eradicated by ex vivo 1B50-1 treatment.

1B50-1 Suppresses the Growth of HCC In Vivo and Eradicates TICs

Next, we examined whether 1B50-1 could have a therapeutic effect on established HCC engraftments by administering 1B50-1 intraperitoneally (i.p.). As shown in Figures 4A–4C, the growth of both Hep-12 and Huh7 cells was dramatically suppressed by 1B50-1 treatment in a dose-dependent manner, although the percentages of positive cells varied greatly between the two cell lines (Table 1). Some of the tumors formed by Hep-12 cells almost completely disappeared following 1B50-1 treatment. The suppression effect of 1B50-1 was also detected on xenografts derived from a HCC primary culture (Figure 4D).

Because 1B50-1 treatment alone retarded tumor growth only to a moderate degree, we examined the therapeutic efficacy of the combination of 1B50-1 and doxorubicin (DXR). By injecting 800 μg 1B50-1 and 1.5 mg/kg DXR i.p. per mouse, the growth of Huh7 engraftments was inhibited by as much as 89.0% compared with the control, representing a further 46.5% inhibition compared with DXR alone (Figures 4E and 4F). A similar effect with combined therapy was also observed for tumor xenografts directly derived from two HCC patients (patient-derived xenograft [PDX]) (Figures 4G and 4H). The survival of mice was also improved following combined therapy in the PDX models (Figures 4I and 4J).

We then analyzed the TICs in the residues of treated Huh7 engraftments. Although the tumor inhibition of 1B50-1 was less effective than DXR, the proportion of 1B50-1$^+$ cells decreased upon antibody treatment, whereas the population of 1B50-1$^+$ cells was significantly enriched after DXR treatment (Figure 4K). Moreover, serial transplantation of 10^4 cells into secondary NOD/SCID mice from tumors that received 1B50-1 treatment formed tumors in two out of 10 mice, while the cells from the control and DXR-treated tumors subsequently formed tumors in nine out of 10 and five out of five injected mice, respectively, with DXR-treated cells developing tumors more rapidly. Notably, only a tiny nodule was found in one out of five mice transplanted with residual cells from an engraftment treated with 1B50-1 plus DXR (Figures 4L and 4M), suggesting TICs were reduced following combined treatment in vivo.

We next detected apoptotic cells by TUNEL assay in the xenografts following 1B50-1 treatment. Consistent with in vitro results, the apoptotic cell percentage increased significantly in both Hep-12 and HuH7 engraftments treated with 800 μg 1B50-1 per mouse (Figures 4N and 4O; Figure S3).

These data demonstrate that 1B50-1 has a therapeutic effect on HCC by targeting TICs, which is augmented by combination with DXR.

The Antigen Recognized by 1B50-1 Is α2δ1, Isoform 5

To identify the antigen recognized by 1B50-1, we performed immunoprecipitation and mass spectrometry analysis using Hep-11 and Hep-12 cells. Unlike in Hep-11 cells, immunoprecipitation of Hep-12 cell lysates with 1B50-1 resulted in several dominant bands observed by SDS-PAGE (Figure 5A). Only the ~150 kDa band was predicted to be a membrane protein with a matched molecular weight of glycosylated α2δ1,

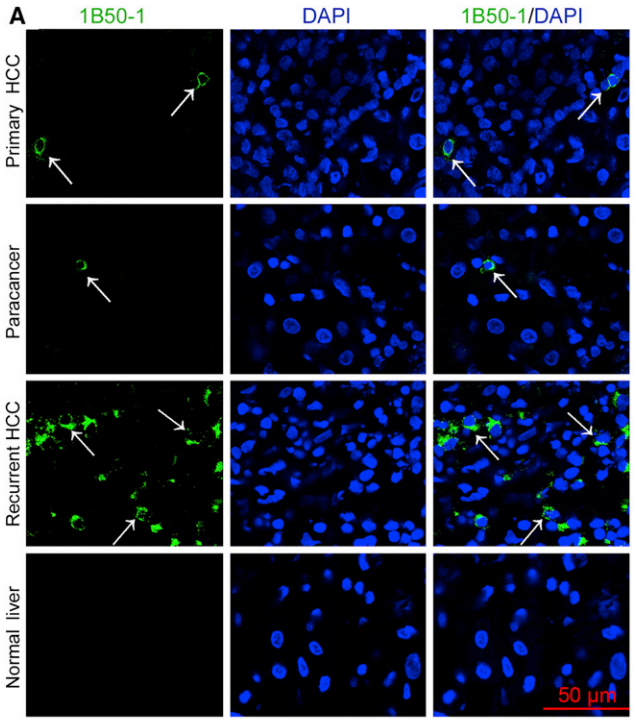

B

Patient	Age (Year)	Gender	Venous thrombosis	AFP (ng/ml)	Tumorigenicity (Tumor)# 1B50-1+	Tumorigenicity (Tumor)# 1B50-1-	Tumorigenicity (PCa)# 1B50-1+	Tumorigenicity (PCa)# 1B50-1-
Case-5	40	Female	Yes	9621	1/1 (10^4)	0/1 (2×10^4)	1/1 (10^4)	0/1 (10^4)
Case-6	70	Male	No	63	1/1 (10^3)	0/1 (2×10^4)	1/1 (2×10^4)	0/1 (2×10^4)
Case-7	55	Male	No	430	1/1 (5×10^3)	0/1 (10^5)	0/1 (10^4)	0/1 (10^5)

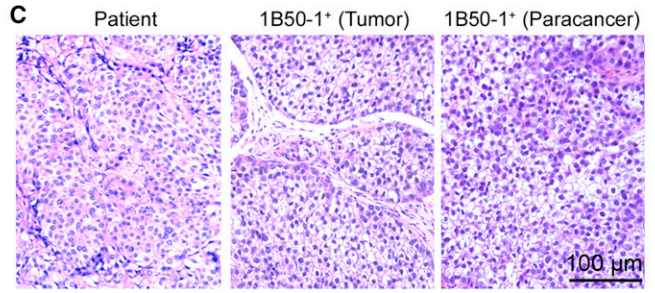

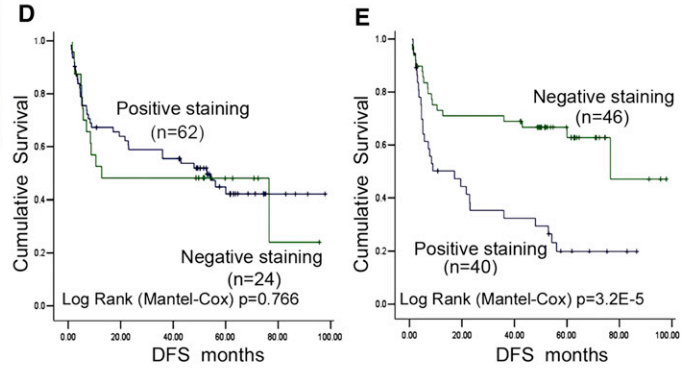

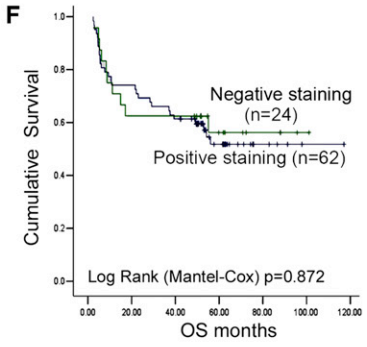

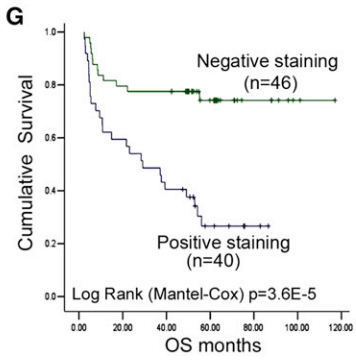

H

Variable		Cases (n)	4-year survival rate (%)	Univariate p value*	Multivariate (Cox-regression) RR (95% CI)	Multivariate (Cox-regression) p value
Gender	Male	75	64.0	0.155	0.732 (0.316-1.697)	0.467
	Female	11	36.4			
Age (Year)	≤60	63	54.0	0.073	1.525 (0.589-3.950)	0.385
	>60	23	78.3			
Cirrhosis	Absent	27	81.5	0.007	0.476 (0.190-1.189)	0.112
	Present	59	50.8			
Size	≤5 cm	46	80.4	0.00005	2.908 (0.917-9.226)	0.070
	>5 cm	40	2.5			
Venous invasion	Absent	64	70.3	0.001	0.457 (0.216-0.967)	0.041
	Present	22	31.8			
1B50-1 (PCa)	Negative	46	80.4	0.00005	0.211 (0.089-0.503)	0.0004
	Positive	40	37.5			
1B50-1 (Ca)	Negative	24	62.5	0.810	1.306 (0.550-3.098)	0.545
	Positive	62	59.7			

Figure 2. Clinical Significance of 1B50-1+ Cells in HCC Patients

(A) Immunohistochemical staining of cryostat sections of primary and recurrent HCC tissues, paracancerous tissues and normal liver with 1B50-1. Nuclei were stained with DAPI. Arrows indicate positive cells.

(B) The tumorigenicity of 1B50-1+ and 1B50-1− cells purified directly from freshly resected HCC and matched paracancerous tissues. #The data are expressed as number of tumors formed/number of sites injected, and the numbers of cell injected are shown in parentheses.

(C) H&E staining of the tumors formed in (B) by 1B50-1+ cells from both the tumor and paracancerous tissues, as well as the original patient HCC tissue (case-5).

(D–G) Kaplan-Meier curves for disease-free (DFS) and overall survival (OS) were compared according to 1B50-1 staining status in HCC tissues (D and F) and the paracancerous tissues (E and G).

(legend continued on next page)

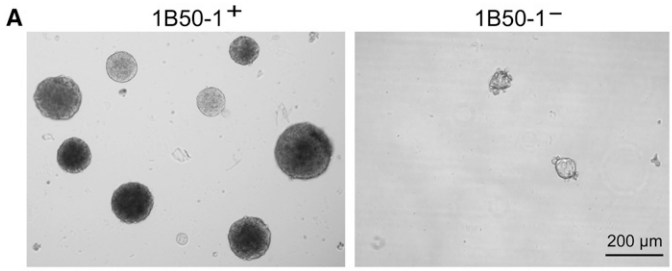

C

Cells	1B50-1 positive		1B50-1 negative	
	10^3	10^2	10^3	10^2
Huh7	5/5	5/5	0/5	0/5
Hep-11	5/5	ND	0/5	ND
Case-5#	3/3	1/3	0/3	0/3
Case-7	3/3	3/3	0/3	0/3

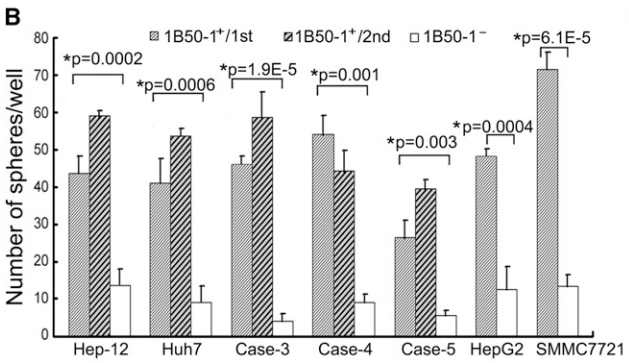

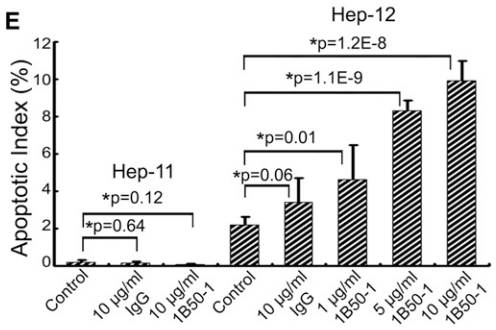

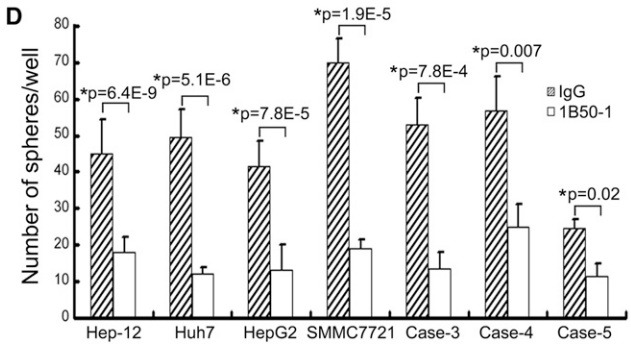

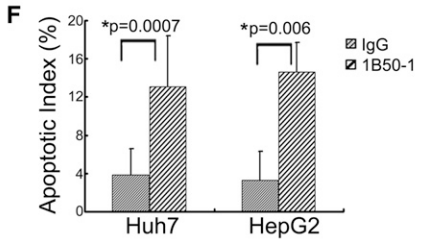

G

Cells	Control		1B50-1	
	10^6	10^5	10^6	10^5
Hep-12	5/5	3/5	0/5	0/5
Huh7	5/5	3/5	0/5	0/5
SMMC7721	3/3	ND	0/3	ND

Figure 3. The Self-Renewal Property of 1B50-1$^+$ HCC Cells and the Effects of 1B50-1 In Vitro

(A) Representative phase contrast micrographs show the spheroids formed by 1B50-1$^+$ and 1B50-1$^-$ HCC cells.

(B) Histograms showing the spheroid forming efficiency of FACS-sorted 1B50-1$^+$ and 1B50-1$^-$ fractions from indicated sources. The ability of the spheres formed by 1B50-1$^+$ cells to form secondary spheroid was also shown (1B50-1$^+$/2nd). One hundred cells per well were plated (n = 6). Spheroids ($\geq$100 μm) were counted under a stereomicroscope.

(C) Tumor formation of serial transplantation assay: 1B50-1$^+$ and 1B50-1$^-$ subsets sorted from xenografted tumors by 1B50-1$^+$ cells in Table 1 and Figure 2B were transplanted s.c. into secondary NOD/SCID mice. #The tumor formed by paracancerous 1B50-1$^+$ cells were used.

(D) Histograms showing the effect of 1B50-1 (10 μg/ml) on spheroid formation of sorted 1B50-1$^+$ cells (n = 6).

(E and F) Histograms showing the effect of 1B50-1 on apoptosis of Hep-11 and Hep-12 cell lines (E) or purified 1B50-1$^+$ subsets from indicated HCC cell lines (F). Cells were treated with 10 μg/ml 1B50-1 for 48 hr in vitro and processed using TUNEL assay followed by flow cytometry.

(G) The tumorigenicity of HCC cells treated with 10 μg/ml 1B50-1 or nonrelated IgG (control) for 48 hr in vitro and subsequently transplanted into NOD/SCID mice.

All error bars indicate SD. *Student's t test. ND, not done.

See also Figure S2.

a composing subunit of a voltage-dependent calcium channel (Figures S4A and S4B). Hence, it was selected for further analysis.

An analysis of α2δ1, which is encoded by *CACNA2D1*, was conducted to examine whether its expression was associated with 1B50-1 staining. qRT-PCR showed that the α2δ1 mRNA

(H) Univariate and multivariate analysis predicts risk factors of poor survival for HCC patients. *Chi-square test. Note: 1B50-1$^+$ staining is defined as the presence of at least one 1B50-1$^+$ cell in a whole cryostat slice, which was screened under a microscope with a 10× lens blindly by two experienced researchers. Negative staining indicates that no 1B50-1$^+$ cells were found. Ca, cancer; PCa, paracancer; RR, relative risk.

See also Table S1.

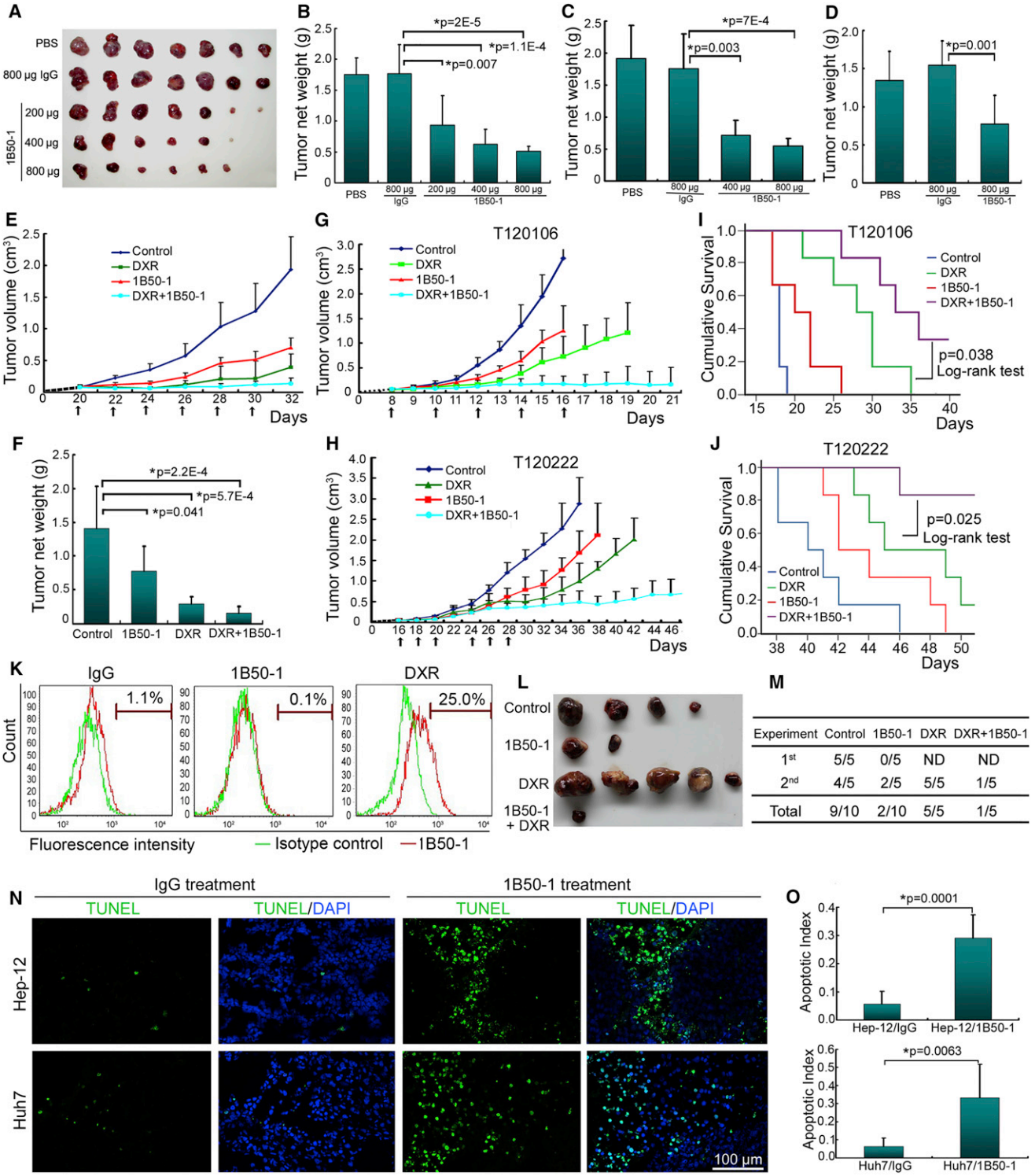

Figure 4. The Therapeutic Effects of 1B50-1 on Established HCC Engraftments in NOD/SCID Mice

(A–D) The mice transplanted s.c. with Hep-12 (A and B, n = 7), Huh7 (C, n = 5), and primary HCC cells (D, n = 5) were injected i.p. with PBS, nonrelated IgG, or 1B50-1 at indicated doses every other day for a total of seven times after the tumors were visible. Tumors were dissected and weighed at experiment termination.

(E and F) Growth curves of Huh7 engraftments treated with 800 μg 1B50-1, 1.5 mg/kg doxorubicin (DXR), or the combination of both, per mouse as indicated by arrows in (E). The histogram in (F) shows the average weight of the dissected tumors (n = 7).

(G and H) Growth curves of two HCC PDX tumors injected i.p. with 800 μg 1B50-1, 1.5 mg/kg DXR, or the combination of both, per mouse as indicated by arrows (n = 6).

(I and J) Kaplan-Meier survival curves of the PDX models in (G) and (H) following the treatments.

(legend continued on next page)

was highly expressed in Hep-12 cells compared with Hep-11 cells (Figure 5B) and in 1B50-1$^+$ subsets compared with their 1B50-1$^-$ counterparts from HCC cell lines and primary tumor-derived cells (Figure 5C). Furthermore, western blot with a commercial α2δ1 mAb showed that Hep-12 cells and 1B50-1$^+$ HCC specimens expressed high levels of α2δ1 protein, while it was undetectable in Hep-11 cells and IB50-1$^-$ paracancerous tissues (Figures 5D and 5E). Additionally, double staining of Hep-12 cells and HCC specimens with 1B50-1 and a rabbit polyclonal α2δ1 antibody confirmed that both antibodies colocalized (Figure 5F).

Because α2δ1 has five isoforms, we determined if 1B50-1 is isoform specific. Double staining (with MYC and 1B50-1 antibodies) of COS-7 cells transiently transfected with each MYC-tagged α2δ1 isoform revealed that 1B50-1 specifically recognized isoform 5, while it weakly cross-reacted with the other four isoforms (Figure 5G). Further PCR cloning and sequencing verified that the mRNA encoding the target protein in 1B50-1$^+$ HCC cells was indeed that of α2δ1 isoform 5 (Figures S4C and S4D). Consistently, skeletal muscle, which expresses isoform 1 of α2δ1, was positively stained by the commercial polyclonal α2δ1 antibody but was negative for 1B50-1 staining (Figure 5F), further suggesting that 1B50-1 specifically recognizes isoform 5 of α2δ1. Finally, knockdown with shRNAs specifically targeting α2δ1 resulted in decreased 1B50-1 staining in Hep-12 cells (Figures 5H–5J). All of these data confirm that the antigen recognized by 1B50-1 is indeed isoform 5 of α2δ1.

The Effects of α2δ1 Knockdown and Overexpression on TIC Properties

If 1B50-1 functions by blocking α2δ1, knockdown of its expression should mimic the effects of 1B50-1 treatment. To validate this hypothesis, we performed RNAi experiments. Knockdown of α2δ1 led to reduced sphere formation, enhanced apoptosis, and decrease of tumorigenic cells among Hep-12 cells (Figures 5K–5M; Figure S4E). In addition, knockdown of α2δ1 in purified 1B50-1$^+$ cells from other HCC cell lines and primary HCC-derived cells reduced sphere formation and tumorigenicity and increased cell apoptosis (Figures 5K, 5L, and 5N).

We also overexpressed α2δ1 isoform 5 in Hep-11 cells and 1B50-1$^-$ populations purified from other HCC cell lines. Although overexpression of α2δ1 did not lead to a significant change in tumorigenicity of Hep-11 cells, it increased hepatosphere-forming efficiency. Similar results were obtained in other 1B50-1$^-$ populations upon α2δ1 overexpression (Figure 5O).

α2δ1 Regulates Calcium Influx in Liver TICs

To determine whether 1B50-1 binding of α2δ1, which is a subunit of a voltage-dependent calcium channel, affects calcium influx, we first measured changes in intracellular calcium concentration ($[Ca^{2+}]_i$) with the Ca^{2+} indicator Fluo-4AM. $[Ca^{2+}]_i$ in Hep-12 cells was significantly higher than that of nontumorigenic Hep-11 cells, as shown by the intensity of fluorescence. Treatment of Hep-12 cells with 10 μg/ml 1B50-1 for 24 hr resulted in a 25.5% decrease of fluorescence intensity, which was statistically significant compared with IgG-treated cells, whereas Hep-11 cells were not affected by 1B50-1 treatment (Figure 6A). Furthermore, analysis of $[Ca^{2+}]_i$ in other HCC cell lines and primary HCC-derived cells revealed that the average $[Ca^{2+}]_i$ level in 1B50-1$^+$ fractions was significantly higher than that of 1B50-1$^-$ subsets, and 1B50-1 treatment resulted in a marked reduction of $[Ca^{2+}]_i$ in 1B50-1$^+$ cells (Figure 6B; Figure S5A). Overexpression of α2δ1 resulted in elevation of $[Ca^{2+}]_i$ in Hep-11 cells (Figure 6C; Figure S5B), whereas knockdown of α2δ1 in Hep-12 cells led to decrease in $[Ca^{2+}]_i$ (Figure 6D). All these data show that α2δ1 plays a role in the calcium influx in 1B50-1$^+$ liver TICs.

Next, we monitored time-dependent changes in $[Ca^{2+}]_i$ in individual cells. Irregular calcium transients were observed in most Hep-12 cells. They appeared more frequently and with more varied intervals in Hep-12 cells compared with Hep-11 cells, in which transients were only observed in approximately 1%–2% of cells (Figures 6E–6G). Calcium transients diminished when extracellular Ca^{2+} was chelated with EGTA and restored when calcium was added into the culture medium (Figures S5C and S5D), suggesting that spontaneous $[Ca^{2+}]_i$ oscillations in TIC-enriched Hep-12 cells depended on the influx of extracellular calcium. Treatment of Hep-12 cells with 1B50-1 did not alter the frequency of spontaneous $[Ca^{2+}]_i$ oscillations, but their amplitude was significantly suppressed (Figures 6H–6J). α2δ1 knockdown in Hep-12 cells gave similar results (Figures 6K and 6L). These data confirm that α2δ1 plays an essential role in calcium oscillations in HCC TICs and that 1B50-1 inhibits the function of α2δ1.

The Hepatosphere-Forming Ability of 1B50-1$^+$ Liver TICs Depends on L- and N-type Calcium Channels

Given that α2δ1 may function through both calcium channel-dependent and independent mechanisms and that multiple calcium channels may be involved in calcium influx, we first determined which calcium channel is involved in the TIC self-renewal regulated by α2δ1 using specific calcium channel blockers. As shown in Figure 6M, the hepatosphere formation ability of 1B50-1$^+$ liver TICs isolated from different HCC cell lines, as well as that of α2δ1-overexpressing Hep-11 cells, was inhibited by L-type and N-type but not T-type calcium channel blockers, indicating that α2δ1 regulates TIC self-renewal through at least L-type and N-type calcium channels.

We then determined whether other subunits of functional voltage-gated calcium channels were present in the TICs by performing RT-PCR analysis of the mRNAs coding for all known 10 α1 subunits and three β subunits of voltage-gated calcium

(K) Residual tumors of (E) were digested into single cells, stained by 1B50-1 after depleting red blood cells, and analyzed by flow cytometry to detect the percentage of 1B50-1$^+$ cells in the residual tumors after treatment.
(L and M) The tumor-initiating ability of the Huh7 engraftment residues after each drug treatment was assayed by retransplanting 10^4 cells with Matrigel into NOD/SCID mouse. The data in (M) are from two independent experiments, and the photograph in (L) shows the dissected tumors of one experiment. ND, not done.
(N and O) Apoptotic cells in engraftments treated with 800 μg 1B50-1 per mouse were detected in situ using the TUNEL assay. The apoptotic index was assessed by the ratio of TUNEL-positive cells/total number of cells from six randomly selected high-power fields (400×). All error bars indicate SD. *Student's t test.
See also Figure S3.

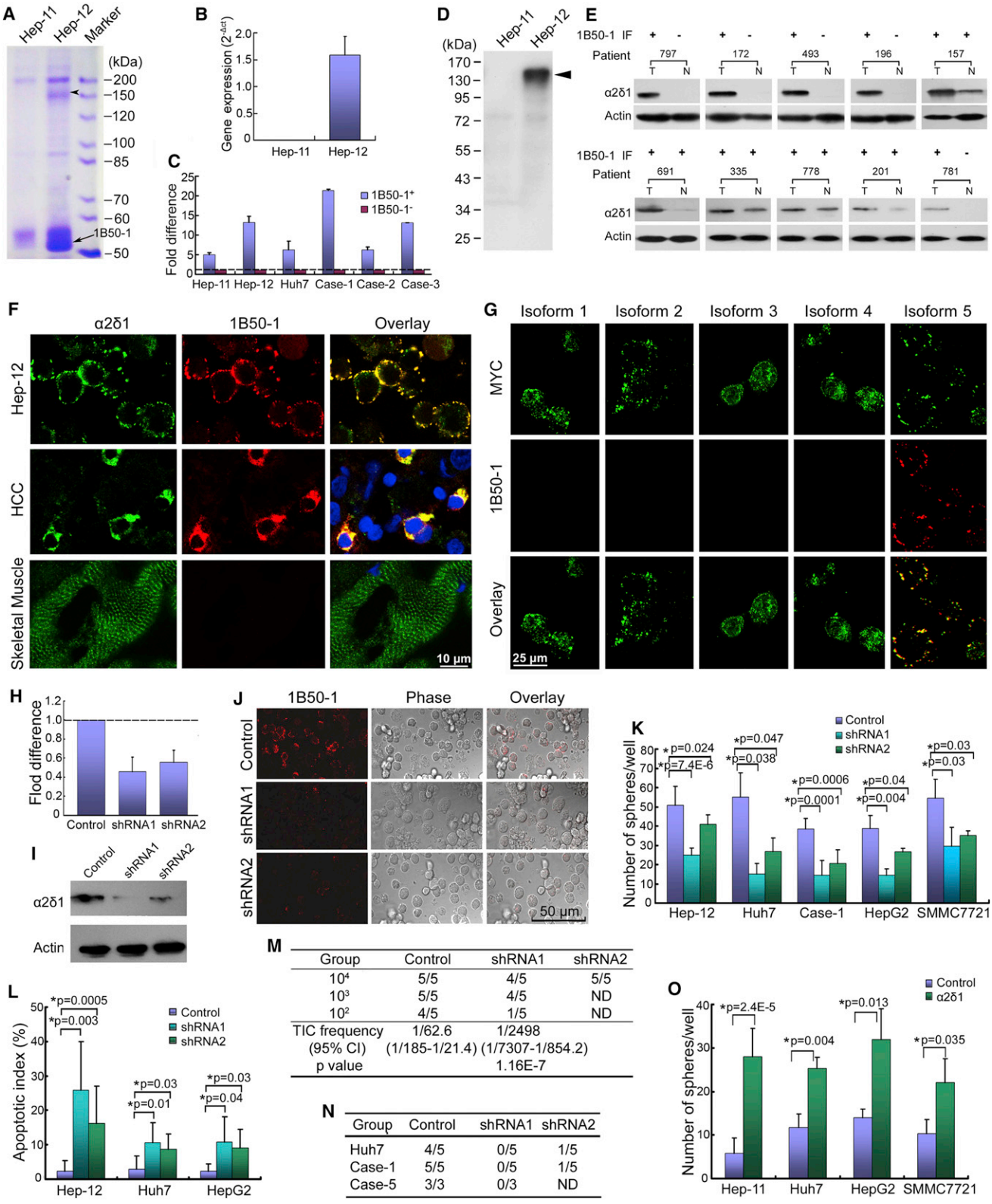

Group	Control	shRNA1	shRNA2
10^4	5/5	4/5	5/5
10^3	5/5	4/5	ND
10^2	4/5	1/5	ND
TIC frequency (95% CI)	1/62.6 (1/185-1/21.4)	1/2498 (1/7307-1/854.2)	
p value		1.16E-7	

Group	Control	shRNA1	shRNA2
Huh7	4/5	0/5	1/5
Case-1	5/5	0/5	1/5
Case-5	3/3	0/3	ND

Figure 5. The Roles of α2δ1 in HCC TICs

(A) SDS-PAGE analysis of 1B50-1 immunoprecipitation products from Hep-11 and Hep-12 cells. The arrowhead indicates the band that was cut out for mass spectrometry analysis.

(B) qRT-PCR analysis of the α2δ1 mRNA level relative to *GAPDH* mRNA level in Hep-11 and Hep-12 cell lines.

(legend continued on next page)

channels. As shown in Figure S5E, the mRNAs encoding α1B, α1C, and α1F subunits were highly expressed in Hep-12 cells compared with Hep-11 cells, while those for α1A, α1D, α1G, α1H, β1, and β3 subunits were equally expressed in both cell lines. Furthermore, when α2δ1 was transfected into Hep-11 cells, the expression of α1B, α1C, and α1F mRNAs was induced. The data were further confirmed with qRT-PCR analysis of α1B, α1C, α1D, and α1F mRNAs in these cells and sorted 1B50-1$^+$ and 1B50-1$^-$ subsets (Figure 6N). These data suggest that the most important subunits of a functional calcium channel do exist in TICs and that α2δ1 could upregulate the expression of α1B, α1C, and α1F subunits.

α2δ1 Knockdown Inhibits ERK1/2 Phosphorylation and Triggers Apoptosis

Because calcium oscillations play a pivotal role in activating signaling cascades that regulate gene transcription and various cell functions, we performed western blots to investigate the molecular mechanisms underlying the effects of 1B50-1 treatment and α2δ1 knockdown. As shown in Figure 7A, the phosphorylation of ERK1/2 in Hep-12 cells was suppressed upon 1B50-1 treatment and α2δ1 knockdown, while both the overall protein and phosphorylation levels of PI3K and AKT were unaffected. Furthermore, consistent with its apoptosis-inducing effects, both 1B50-1 treatment and α2δ1 shRNA knockdown resulted in downregulation of the antiapoptotic protein BCL2 and upregulation of BAX and BAD, as well as activation of caspases 3, 8, and 9, as shown by increased levels of cleaved proteins. Notably, the expression of ABCG2 and BMI1, which is important for stem cell self-renewal (Chiba et al., 2008), was also downregulated.

Next, we validated the aforementioned data in cells purified from primary HCC-derived cells by western blot analysis of some representative proteins. Compared with their 1B50-1$^-$ counterparts, 1B50-1$^+$ cells expressed higher levels of ABCG2, BMI1, BCL2, and OCT4, as well as phosphorylated ERK1/2 (p-ERK1/2). 1B50-1 treatment of 1B50-1$^+$ cells resulted in downregulation of these proteins and dephosphorylation of ERK1/2 (Figure 7B).

It is important to note that the expression of those proteins downregulated by α2δ1 blocking, such as BMI1, OCT4, ABCG2, BCL2, and p-ERK1/2, was upregulated upon α2δ1 overexpression (Figure 7C).

An ERK1/2 Inhibitor, U0126, Mimics the Effects of α2δ1 Blocking

The aforementioned findings indicate that the MAPK pathway regulates liver TIC properties. To test this hypothesis, we treated Hep-12 cells and 1B50-1$^+$ fractions from other HCC cell lines with an ERK1/2 inhibitor, U0126. The expression of BMI1, OCT4, ABCG2, and BCL2 were downregulated by 10 μM U0126 treatment for 48 hr (Figure 7D). The hepatosphere formation of Hep-12 cells, purified 1B50-1$^+$ subsets from various HCC cell lines, and α2δ1-overexpressing Hep-11 cells was also suppressed upon U0126 treatment (Figures 7E and 7F). These data suggest that ERK1/2 inhibition mimics the effects of 1B50-1 treatment and α2δ1 knockdown, suggesting that ERK1/2 activity is essential for the maintenance of HCC TIC properties.

DISCUSSION

The TICs are proposed to be responsible for tumor recurrence according to the cancer stem cell hypothesis (Visvader and Lindeman, 2012). Here, we identified a population of HCC TIC expressing α2δ1 in primary HCC and some surgical margins using a mAb, 1B50-1, generated against the recurrent HCC-derived cell line Hep-12, suggesting these α2δ1$^+$ TICs might be the cell of origin for HCC recurrence.

The differentiation capability of 1B50-1$^+$ cells from the recurrent HCC-originated Hep-12 cells, which have a block of differentiation capacity in vitro or in vivo (Xu et al., 2010), is quite different from those purified from primary HCC-derived cells in that they established equilibrium at a different percentage of 1B50-1$^+$ cells. This observation indicates that, during tumor progression, the same TIC population undergoes clonal evolution under selection pressures that enable these cells to acquire additional characteristics and to remain in a more stable state.

α2δ1 was previously proposed as a potential hepatic progenitor cell marker (Yovchev et al., 2007). We confirmed that 1B50-1 recognized many cells in resected mouse liver as well as in colony-forming units of normal mouse liver (data not shown).

(C) qRT-PCR analysis of the α2δ1 mRNA level in purified 1B50-1$^+$ fractions relative to that in their 1B50-1$^-$ counterparts of indicated sources.
(D and E) Western blot analysis with a α2δ1 mAb in HCC cell lines (D) or paired tumor (T) and paracancerous (N) tissues from HCC patients (E). The corresponding 1B50-1 immunofluorescence staining status (1B50-1 IF) is also given above each lane for comparison. +, positive; −, negative.
(F) Cultured Hep-12 cells, cryostat sections of HCC tissue and skeletal muscle were fixed with methanol, double-stained with 1B50-1 and a rabbit polyclonal α2δ1 antibody, and observed under a confocal microscope. The HCC tissue and the skeletal muscle were also counterstained with DAPI.
(G) Immunofluorescent staining of COS-7 cells transiently transfected with indicated MYC-tagged isoform of α2δ1 with MYC and 1B50-1 antibodies without fixation.
(H and I) α2δ1 mRNA (H) and protein (I) levels of Hep-12 cells stably infected with lentivirus harboring scramble (control) or shRNA1 or shRNA2 targeting α2δ1.
(J) Hep-12 cells stably infected with indicated lentivirus were immunostained by 1B50-1.
(K) Histogram showing the sphere-forming ability of purified 1B50-1$^+$ subsets after α2δ1 knockdown. Sorted 1B50-1$^+$ cells were incubated with indicated lentivirus for 4 hr, and were plated at 100 cells per well (n = 6).
(L) Sorted 1B50-1$^+$ cells were infected with indicated lentivirus and cultured in serum-free medium for 72 hr, and apoptotic cells were detected by flow cytometry analysis of TUNEL-stained cells.
(M) Hep-12 cells stably infected with indicated lentivirus were transplanted s.c. in NOD/SCID mice at indicated numbers to assay their tumorigenicity.
(N) The tumorigenicity of 1B50-1$^+$ cells purified from indicated sources after α2δ1 shRNA knockdown. 1B50-1$^+$ cells were incubated with indicated lentivirus for 4 hr, and 1,000 cells per mouse were injected.
(O) The sphere-forming ability of sorted 1B50-1$^-$ cells infected with α2δ1 (isoform 5) lentivirus (100 cells per well plated, n = 6). All error bars indicate SD. *Student's t test. ND, not done.
See also Figure S4.

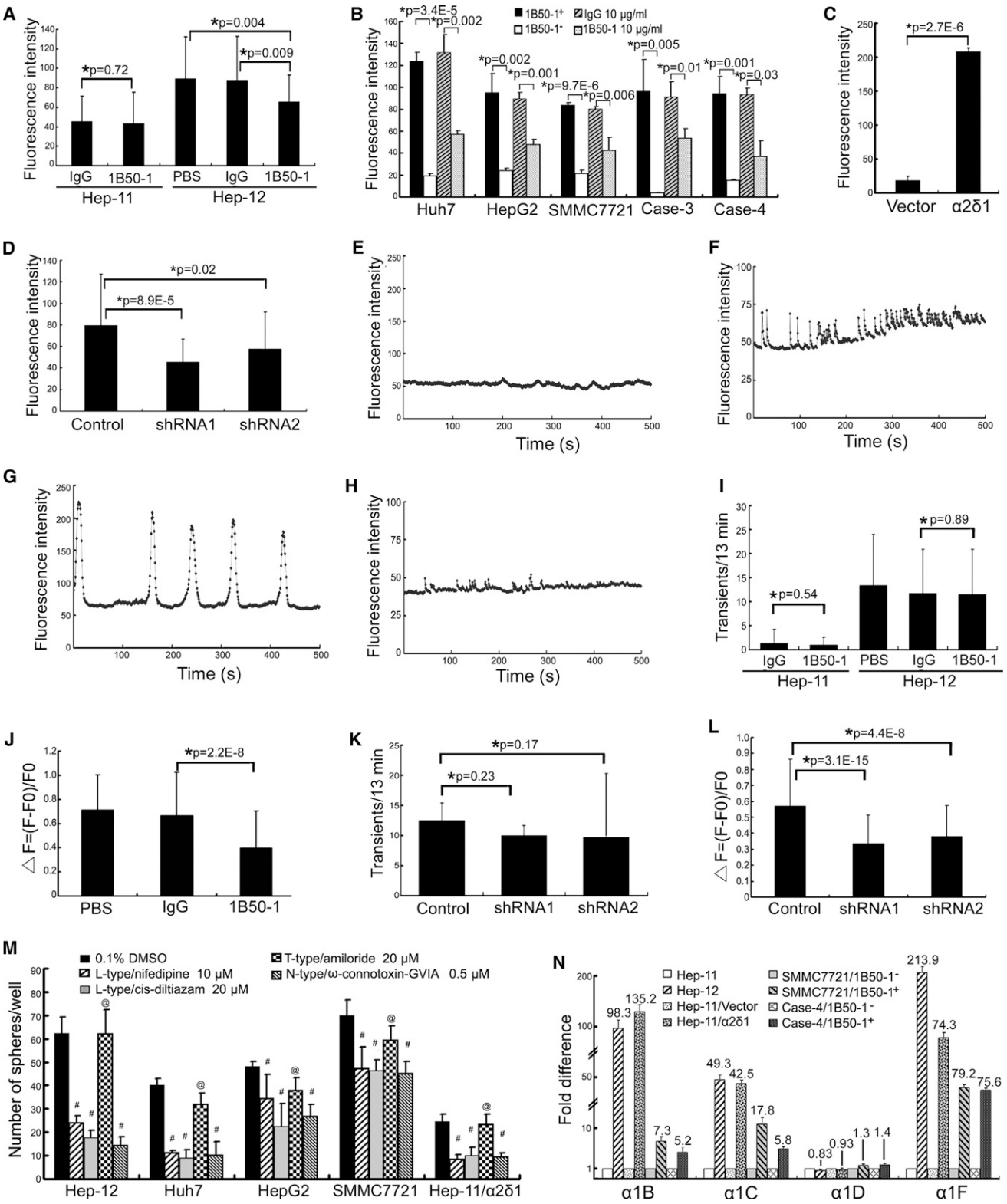

Figure 6. Characterization of Calcium Influx in 1B50-1$^+$ TICs

(A) $[Ca^{2+}]_i$ levels in Hep-11 and Hep-12 cells after treated with IgG or 1B50-1 at 10 μg/ml for 24 hr measured by the fluorescence intensity using confocal microscopy after cells were loaded with Fluo-4AM.

(B) $[Ca^{2+}]_i$ levels in 1B50-1$^+$ and their 1B50-1$^-$ counterparts, as well as in 1B50-1$^+$ subsets treated with IgG or 1B50-1 at 10 μg/ml for 24 hr measured by flow cytometry.

(legend continued on next page)

Its identification as a TIC marker here demonstrates TICs' close correlation with normal liver progenitors. Furthermore, our inability to find cells reacted with 1B50-1 in normal human liver specimens is consistent with the notion that liver progenitors are rare and are not readily detectable in human normal adult liver (Darwiche and Petersen, 2010). Finally, the finding that the cells detected by 1B50-1 in paracancerous tissues also have TIC properties may explain why those patients who have undergone hepatectomy still relapse, and this could have prognostic value. This finding also indicates that specific therapeutic strategies to eradicate these cells should be used for HCC patients with $\alpha2\delta1^+$ cells at the surgical margins.

Our data demonstrate that 1B50-1 has a therapeutic effect on HCC by targeting TICs. Of course, ideally, tumors will disappear when TICs are disrupted completely, according to the TIC hypothesis. However, it is difficult to obtain complete pharmacokinetic control, especially in vivo (as shown by this study and many others; Haraguchi et al., 2010; Visvader and Lindeman, 2012), with an antibody alone, most likely because of inefficient penetration of the antibody to the cells inside the tumor mass and because of the presence of other transit-amplifying tumorigenic cells. Instead, combination therapy of 1B50-1 with other anti-HCC drugs such as DXR, which most likely disrupt TICs and fast-proliferating non-TICs, respectively, would be required to achieve a drastic regression, as demonstrated here.

The target of 1B50-1 was identified and validated as isoform 5 of α2δ1, a subunit of voltage-gated calcium channel complexes (De Jongh et al., 1990; Eroglu et al., 2009). Currently, little is known about the expression pattern and specific function of isoform 5 of α2δ1, although other members of the α2δ family have been extensively investigated. Here, we reveal an essential role of α2δ1 isoform 5 for the modulation of calcium influx and the maintenance of many HCC TIC properties. In addition, it is undetectable in most normal tissues, so cytotoxicity unlikely would be a concern. Hence, α2δ1 isoform 5 could serve as a therapeutic target for the development of drugs against HCC that specifically eradicate TICs.

Our study identified the roles of α2δ1 isoform 5 in liver TICs were related to its calcium influx regulation function through L- and N-type voltage-gated calcium channels. However, the activation of voltage-dependent calcium channels is regulated by polarization and depolarization of membranes, which are often caused by influx of cations. Polarization/depolarization-related signaling pathways and some other calcium channels, such as nicotinic acetylcholine receptors, are also found to be related to tumorigenesis (Hung et al., 2008; Lee et al., 2010). It would be interesting to determine if these molecules are also highly expressed in $\alpha2\delta1^+$ liver TICs and, if so, what the roles are of these molecules in the maintenance of TIC properties.

We identified p-ERK1/2 as a key downstream target of α2δ1 function in liver TICs. This finding is consistent with a previous report that signaling to the nucleus by an L-type calcium channel is transduced through the MAPK pathway (Dolmetsch et al., 2001). Because other signaling pathways, such as the noncanonical Wnt pathway, may also be involved in calcium signaling (MacLeod et al., 2007), further studies are needed to clarify whether these signaling pathways are also involved in the maintenance of cancer stem cell-like properties of HCC TICs by α2δ1.

Spontaneous calcium oscillations occur in cells originating from excitable tissues, such as muscle and neuronal tissues, but they also occur in embryonic stem cells, mesenchymal stem cells, immature dendritic cells, and G0/G1-phase cells, although the regulatory mechanisms and biological functions have not been elucidated in many cases (Ferreira-Martins et al., 2009; Kapur et al., 2007; Vukcevic et al., 2010). $[Ca^{2+}]_i$ oscillations, one of the major forms of calcium signaling, can promote the expression of specific genes, and this is related to the amplitude and duration of calcium transients, possibly by keeping transcription factors in the nucleus at high enough levels to bind enhancer sites and initiate transcription (Dolmetsch et al., 1997; Dolmetsch et al., 1998; Vukcevic et al., 2010). Here, we observed that spontaneous $[Ca^{2+}]_i$ oscillations were present in HCC TICs and were controlled by calcium influx. Because many TIC properties, such as self-renewal, tumorigenicity, and survival, were affected by 1B50-1 treatment and knockdown of α2δ1 and because these treatments resulted in changes in gene expression and a strong decrease in the amplitude of $[Ca^{2+}]_i$ oscillations, we propose that α2δ1 is involved in "amplitude-encoding" signals that maintain the properties of HCC TICs and that inhibition of this signaling could serve as a therapeutic strategy for HCC.

EXPERIMENTAL PROCEDURES

Cell Lines and Clinical Samples

The HCC cell lines Hep-11, Hep-12, HuH7, SMMC-7721, and HepG2 were cultured in RPMI 1640 medium supplemented with 10% fetal bovine serum,

(C) $[Ca^{2+}]_i$ levels in Hep-11 cells after α2δ1 overexpression measured by flow cytometry.
(D) $[Ca^{2+}]_i$ levels in Hep-12 cells following α2δ1 knockdown measured by confocal microscopy.
(E–G) Representative recordings of the fluorescence of individual cells plotted as a function of time showing the change of $[Ca^{2+}]_i$ in the majority of Hep-11 (E) and Hep-12 cells (F). A representative type of $[Ca^{2+}]_i$ oscillation for a minor Hep-11 population was shown in (G).
(H) A representative recording of $[Ca^{2+}]_i$ change with time in Hep-12 cells treated with 1B50-1 at 10 μg/ml for 24 hr.
(I) The frequency of $[Ca^{2+}]_i$ oscillations in indicated cells treated with IgG or 1B50-1 at 10 μg/ml for 24 hr.
(J) The effect of 1B50-1 treatment (10 μg/ml for 24 hr) on the amplitude of $[Ca^{2+}]_i$ oscillations in Hep-12 cells.
(K and L) $[Ca^{2+}]_i$ oscillation frequency (K) and amplitudes (L) in Hep-12 cells after α2δ1 stable knockdown.
(M) The effects of specific calcium channel blockers on spheroid formation were tested using FACS-purified $1B50\text{-}1^+$ cells from indicated sources or α2δ1-overexpressing Hep-11 cells (100 cells per well plated, n = 6).
(N) qRT-PCR analysis of the mRNAs encoding some α1 calcium channel subunits in indicated cells. The fold difference of Hep-12, Hep-11/α2δ1, and $1B50\text{-}1^+$ subsets was calculated over the level of each gene in Hep-11, Hep-11/Vector, and $1B50\text{-}1^-$ cells, respectively. Error bars in all panels indicate SD. The data in (I) through (L) are the mean of 40 cells for each group of four independent experiments.
*, #, and @, Student's t test; $^{\#}p < 0.05$, and $^{@}p > 0.05$ versus 0.1% DMSO.
See also Figure S5.

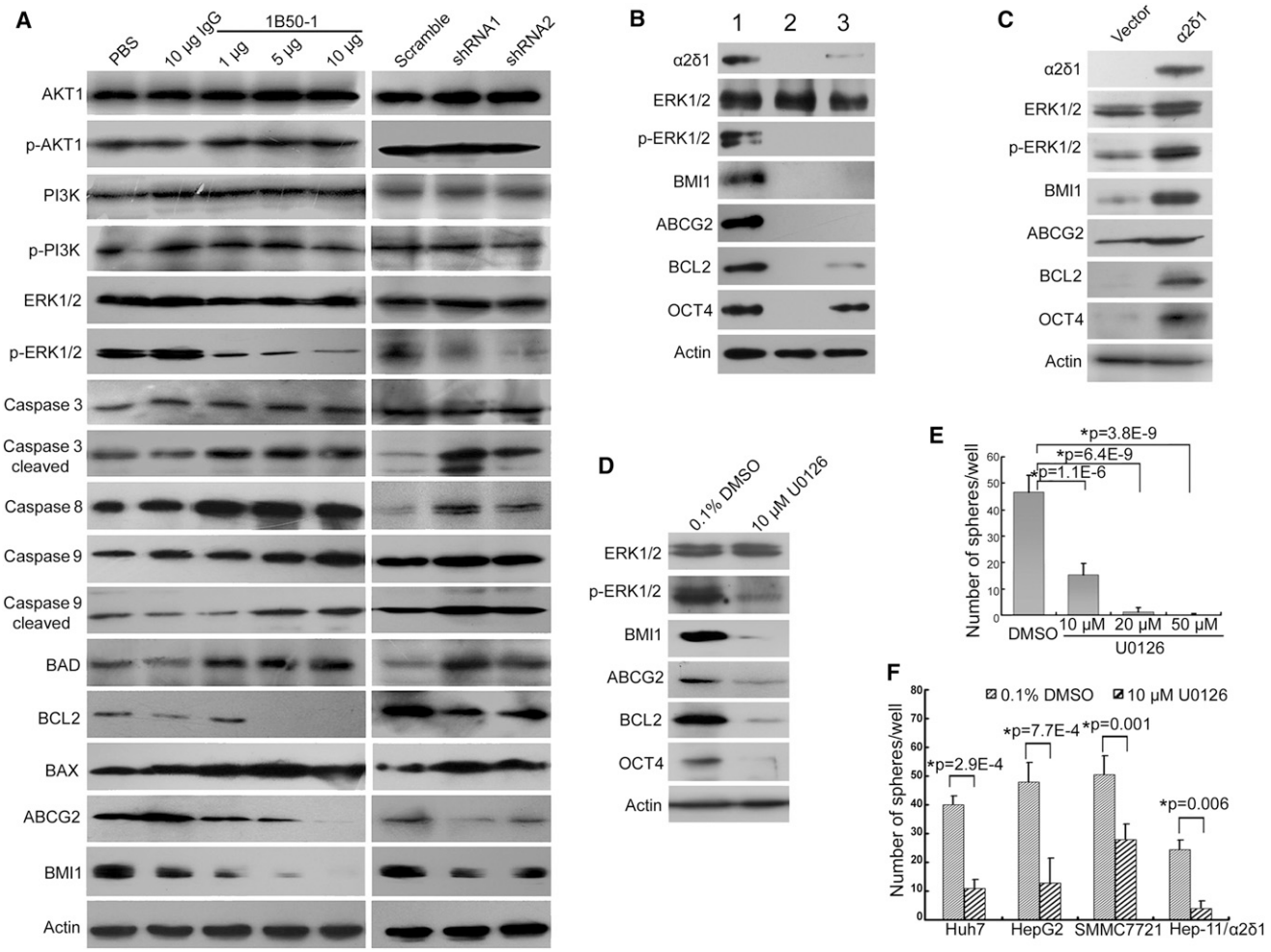

Figure 7. Molecular Mechanisms Underlying the Effects of α2δ1 Blocking

(A) Western blot analysis using lysates of Hep-12 cells treated with IgG or 1B50-1 at indicated doses (per ml) for 48 hr or stable pools infected with lentivirus harboring scramble or shRNA1 or shRNA2 targeting α2δ1.

(B) Western blot analysis using lysates of 1B50-1$^+$ (lane 1), 1B50-1$^-$ (lane 2), and 1B50-1$^+$ cells treated with 10 μg/ml 1B50-1 for 48 hr (lane 3). 1B50-1 fractions were sorted from Case-4 HCC-derived cells.

(C) Western blot analysis to detect the change of representative molecules associated with HCC TICs in Hep-11 cells after α2δ1 (isoform 5) overexpression.

(D) Western blot results show the expression of HCC TIC-related molecules in Hep-12 cells treated with U0126 for 48 hr.

(E) The sphere-forming ability of Hep-12 cells treated with an ERK1/2 inhibitor, U0126.

(F) The effect of U0126 on the sphere-forming ability of sorted 1B50-1$^+$ cells from indicated sources and α2δ1-overexpressing Hep-11 cells. One hundred cells per well were plated (n = 6). All error bars indicate SD. *Student's t test.

100 U/ml penicillin, and 100 μg/ml streptomycin (Invitrogen, Grand Island, NY, USA) in a humidified atmosphere of 5% CO_2 at 37°C.

Primary HCC specimens and matched adjacent normal tissues were collected and snap-frozen into liquid nitrogen from patients who received a hepatectomy with written informed consent. Some fresh HCC tissues were mechanically minced and collagenase IV digested, followed by FACS or primary culture in RPMI 1640 medium containing 10% fetal bovine serum and expansion after removal of fibroblasts. The PDX models were established using mechanically minced fresh HCC specimens. Acquisition and use of these tissues were approved by the Ethics Committee of Peking University Cancer Hospital.

Antibody Production

Subtractive immunization was used to generate antibodies recognizing the epitopes specifically enriched in Hep-12 cells. In brief, mice were immunized with Hep-11 cells, administered 200 mg/kg cyclophosphamide (Sigma-Aldrich, St. Louis, MO, USA), and boosted three times with Hep-12 cells. Fusion, hybridoma screening, antibody production, and purification were performed using standard protocols.

Cell Labeling and Flow Cytometry Analysis

For flow cytometry analysis or FACS, cells were dispersed, labeled, and analyzed as previously described (Xu et al., 2010). 1B50-1 was directly labeled with PE-Cy5 or fluorescein using the respective Lightning conjugation kits following the vendor's protocol (Innova Biosciences Ltd., Cambridge, UK).

Tumorigenicity Assay in NOD/SCID Mice

For the tumorigenicity assay, various numbers of FACS-purified cells were suspended in 50 μl of a 1:1 mix of plain RPMI 1640 and Matrigel (BD Biosciences, Bedford, MA, USA) and transplanted s.c. into the armpit of 4- to 6-week-old NOD/SCID mice (Vitalriver, Beijing, China). Tumor formation was monitored weekly.

To test the therapeutic effect of 1B50-1, cells were s.c. injected into the back of 4- to 6-week-old NOD/SCID mice (2×10^6 cells per mouse). When all the tumors were visible, mice with comparably sized tumors were randomly separated into control and treatment groups and injected i.p. with PBS, nonrelated IgG, 1B50-1, or DXR. The tumor volume was determined using the formula $V = L \times W^2 \times 0.5$, where L and W represent the largest and the smallest diameters, respectively.

All animal experiments were performed in accordance with the National Institutes of Health Guide for the Care and Use of Laboratory Animals with protocols approved by the Animal Care and Use Committee at Peking University Cancer Hospital.

Immunohistochemistry Staining

Frozen tissues were sectioned with a cryostat and fixed with methanol for 30 s. After blocking with 5% nonfat milk in PBS, slides were incubated with 1B50-1 mAb alone or combined with a polyclonal antibody against α2δ1 (Catalog #HPA008213, Sigma, St. Louis, MO, USA) at 4°C overnight, followed by reaction with fluorescein isothiocyanate (FITC)-goat antimouse IgG or both FITC-goat antimouse IgG and rhodamine-goat antirabbit IgG. Nuclei were stained with 4,6-diamidino-2-phenylindole dihydrochloride (DAPI; Polysciences, Warrington, PA, USA) at 0.5 μg/ml. Specimens were mounted in 90% glycerol/PBS containing 2.5% 1, 4-diazabicyclo(2,2,2)octane. Slides were examined with a Leica SP5 confocal microscope (Leica, Wetzlar, Germany).

Sphere Formation Assay

To assay sphere formation efficiency, cells were plated in Ultra Low Attachment 96-well plates (Corning Incorporated Life Sciences, Acton, MA, USA) and cultured in Dulbecco's modified Eagle's medium/F12 (Invitrogen) supplemented with B27 (Invitrogen), 20 ng/ml epidermal growth factor, 20 ng/ml basic fibroblast growth factor (Peprotech), 10 ng/ml hepatocyte growth factor (Peprotech, Rocky Hill, NJ, USA), and 1% methylcellulose (Sigma). Cells were incubated in a CO_2 incubator for 2–3 weeks, and spheres were counted under a stereomicroscope (Olympus, Tokyo, Japan).

Intracellular Calcium Measurement

For the confocal laser scanning microscope method, cells were rinsed twice with warmed Tyrode's solution (140 mM NaCl, 5.0 mM KCl, 1.0 mM $MgCl_2$, 5.5 mM glucose, 10 mM HEPES, 1.8 mM $CaCl_2$, pH 7.2) and labeled with Fluo-4/AM in Tyrode's solution for 15 min at room temperature (RT). After washing, fluorescence was measured at RT using a Zeiss confocal imaging system with a 40× water immersion lens (Carl Zeiss, Jena, Germany). A total of 500 images for each field were captured at intervals of 1.56 s, and the fluorescence was quantified over all the cells in three to six random fields using ImageJ software (http://rsb.info.nih.gov/ij/). The change in $[Ca^{2+}]_i$ was expressed as $\Delta F = (F - F0)/F0$, where F = fluorescence intensity and F0 = resting fluorescence.

For flow cytometry measurement of $[Ca^{2+}]_i$ level, trypsin-digested cells were loaded with Fluo-4/AM as described earlier and analyzed with a flow cytometer.

Statistical Analysis

Using the SPSS 13.0 software, the significance of differences was determined with a double-sided Student's t test or a χ^2 test unless otherwise specified. Tumorigenic cell frequency was calculated based on extreme limiting dilution analysis using the webtool at http://bioinf.wehi.edu.au/software/elda/ (Hu and Smyth, 2009). $p \leq 0.05$ was considered statistically significant.

SUPPLEMENTAL INFORMATION

Supplemental Information includes five figures, one table, and Supplemental Experimental Procedures and can be found with this article online at http://dx.doi.org/10.1016/j.ccr.2013.02.025.

ACKNOWLEDGMENTS

Thanks are given to Professor Cheng Qian for providing the Huh7 cell line and to the FACS Core Facility of Peking University Cancer Hospital for performing FACS assays. This work was supported by the National Basic Research Program of China (the "973" Program, No. 2010CB529402), National Natural Science Foundation of China (grant numbers 81071733 and 31221002), the "863" Project (2007AA02Z133), Beijing NSF (5122012), and Beijing Outstanding Talents Training Funds in Health Sciences (grant No. 2011-2-24). Y.C. is an employee of Genzyme, a Sanofi Company.

Received: September 5, 2012
Revised: December 12, 2012
Accepted: February 27, 2013
Published: April 15, 2013

REFERENCES

Alison, M.R., Lim, S.M., and Nicholson, L.J. (2011). Cancer stem cells: problems for therapy? J. Pathol. *223*, 147–161.

Brooks, P.C., Lin, J.M., French, D.L., and Quigley, J.P. (1993). Subtractive immunization yields monoclonal antibodies that specifically inhibit metastasis. J. Cell Biol. *122*, 1351–1359.

Chiba, T., Kita, K., Zheng, Y.-W., Yokosuka, O., Saisho, H., Iwama, A., Nakauchi, H., and Taniguchi, H. (2006). Side population purified from hepatocellular carcinoma cells harbors cancer stem cell-like properties. Hepatology *44*, 240–251.

Chiba, T., Miyagi, S., Saraya, A., Aoki, R., Seki, A., Morita, Y., Yonemitsu, Y., Yokosuka, O., Taniguchi, H., Nakauchi, H., and Iwama, A. (2008). The polycomb gene product BMI1 contributes to the maintenance of tumor-initiating side population cells in hepatocellular carcinoma. Cancer Res. *68*, 7742–7749.

Clarke, M.F., Dick, J.E., Dirks, P.B., Eaves, C.J., Jamieson, C.H., Jones, D.L., Visvader, J., Weissman, I.L., and Wahl, G.M. (2006). Cancer stem cells—perspectives on current status and future directions: AACR Workshop on cancer stem cells. Cancer Res. *66*, 9339–9344.

Darwiche, H., and Petersen, B.E. (2010). Biology of the adult hepatic progenitor cell: "ghosts in the machine". Prog. Mol. Biol. Transl. Sci. *97*, 229–249.

De Jongh, K.S., Warner, C., and Catterall, W.A. (1990). Subunits of purified calcium channels. Alpha 2 and delta are encoded by the same gene. J. Biol. Chem. *265*, 14738–14741.

Deonarain, M.P., Kousparou, C.A., and Epenetos, A.A. (2009). Antibodies targeting cancer stem cells: a new paradigm in immunotherapy? MAbs *1*, 12–25.

Dolmetsch, R.E., Lewis, R.S., Goodnow, C.C., and Healy, J.I. (1997). Differential activation of transcription factors induced by Ca2+ response amplitude and duration. Nature *386*, 855–858.

Dolmetsch, R.E., Xu, K., and Lewis, R.S. (1998). Calcium oscillations increase the efficiency and specificity of gene expression. Nature *392*, 933–936.

Dolmetsch, R.E., Pajvani, U., Fife, K., Spotts, J.M., and Greenberg, M.E. (2001). Signaling to the nucleus by an L-type calcium channel-calmodulin complex through the MAP kinase pathway. Science *294*, 333–339.

Eroglu, C., Allen, N.J., Susman, M.W., O'Rourke, N.A., Park, C.Y., Ozkan, E., Chakraborty, C., Mulinyawe, S.B., Annis, D.S., Huberman, A.D., et al. (2009). Gabapentin receptor alpha2delta-1 is a neuronal thrombospondin receptor responsible for excitatory CNS synaptogenesis. Cell *139*, 380–392.

Ferreira-Martins, J., Rondon-Clavo, C., Tugal, D., Korn, J.A., Rizzi, R., Padin-Iruegas, M.E., Ottolenghi, S., De Angelis, A., Urbanek, K., Ide-Iwata, N., et al. (2009). Spontaneous calcium oscillations regulate human cardiac progenitor cell growth. Circ. Res. *105*, 764–774.

Haraguchi, N., Ishii, H., Mimori, K., Tanaka, F., Ohkuma, M., Kim, H.M., Akita, H., Takiuchi, D., Hatano, H., Nagano, H., et al. (2010). CD13 is a therapeutic target in human liver cancer stem cells. J. Clin. Invest. *120*, 3326–3339.

Hoey, T., Yen, W.-C., Axelrod, F., Basi, J., Donigian, L., Dylla, S., Fitch-Bruhns, M., Lazetic, S., Park, I.-K., Sato, A., et al. (2009). DLL4 blockade inhibits tumor growth and reduces tumor-initiating cell frequency. Cell Stem Cell *5*, 168–177.

Hu, Y., and Smyth, G.K. (2009). ELDA: Extreme limiting dilution analysis for comparing depleted and enriched populations in stem cell and other assays. J. Immunol. Methods *347*, 70–78.

Hung, R.J., McKay, J.D., Gaborieau, V., Boffetta, P., Hashibe, M., Zaridze, D., Mukeria, A., Szeszenia-Dabrowska, N., Lissowska, J., Rudnai, P., et al. (2008).

A susceptibility locus for lung cancer maps to nicotinic acetylcholine receptor subunit genes on 15q25. Nature *452*, 633–637.

Jin, L., Lee, E.M., Ramshaw, H.S., Busfield, S.J., Peoppl, A.G., Wilkinson, L., Guthridge, M.A., Thomas, D., Barry, E.F., Boyd, A., et al. (2009). Monoclonal antibody-mediated targeting of CD123, IL-3 receptor alpha chain, eliminates human acute myeloid leukemic stem cells. Cell Stem Cell *5*, 31–42.

Kapur, N., Mignery, G.A., and Banach, K. (2007). Cell cycle-dependent calcium oscillations in mouse embryonic stem cells. Am. J. Physiol. Cell Physiol. *292*, C1510–C1518.

Lee, C.-H., Huang, C.-S., Chen, C.-S., Tu, S.-H., Wang, Y.-J., Chang, Y.-J., Tam, K.-W., Wei, P.-L., Cheng, T.-C., Chu, J.-S., et al. (2010). Overexpression and activation of the α9-nicotinic receptor during tumorigenesis in human breast epithelial cells. J. Natl. Cancer Inst. *102*, 1322–1335.

Lee, T.K., Castilho, A., Cheung, V.C., Tang, K.H., Ma, S., and Ng, I.O. (2011). CD24+ Liver Tumor-Initiating Cells Drive Self-Renewal and Tumor Initiation through STAT3-Mediated NANOG Regulation. Cell Stem Cell *9*, 50–63.

Llovet, J.M., and Bruix, J. (2008). Molecular targeted therapies in hepatocellular carcinoma. Hepatology *48*, 1312–1327.

Ma, S., Tang, K.H., Chan, Y.P., Lee, T.K., Kwan, P.S., Castilho, A., Ng, I., Man, K., Wong, N., To, K.F., et al. (2010). miR-130b Promotes CD133(+) liver tumor-initiating cell growth and self-renewal via tumor protein 53-induced nuclear protein 1. Cell Stem Cell *7*, 694–707.

MacLeod, R.J., Hayes, M., and Pacheco, I. (2007). Wnt5a secretion stimulated by the extracellular calcium-sensing receptor inhibits defective Wnt signaling in colon cancer cells. Am. J. Physiol. Gastrointest. Liver Physiol. *293*, G403–G411.

Mishra, L., Banker, T., Murray, J., Byers, S., Thenappan, A., He, A.R., Shetty, K., Johnson, L., and Reddy, E.P. (2009). Liver stem cells and hepatocellular carcinoma. Hepatology *49*, 318–329.

Rappa, G., Fodstad, O., and Lorico, A. (2008). The stem cell-associated antigen CD133 (Prominin-1) is a molecular therapeutic target for metastatic melanoma. Stem Cells *26*, 3008–3017.

Rasmussen, N., and Ditzel, H.J. (2009). Scanning the cell surface proteome of cancer cells and identification of metastasis-associated proteins using a subtractive immunization strategy. J. Proteome Res. *8*, 5048–5059.

Rosen, J.M., and Jordan, C.T. (2009). The increasing complexity of the cancer stem cell paradigm. Science *324*, 1670–1673.

Sell, S., and Leffert, H.L. (2008). Liver cancer stem cells. J. Clin. Oncol. *26*, 2800–2805.

Shackleton, M., Quintana, E., Fearon, E.R., and Morrison, S.J. (2009). Heterogeneity in cancer: cancer stem cells versus clonal evolution. Cell *138*, 822–829.

Todaro, M., Alea, M.P., Di Stefano, A.B., Cammareri, P., Vermeulen, L., Iovino, F., Tripodo, C., Russo, A., Gulotta, G., Medema, J.P., and Stassi, G. (2007). Colon cancer stem cells dictate tumor growth and resist cell death by production of interleukin-4. Cell Stem Cell *1*, 389–402.

Visvader, J.E. (2011). Cells of origin in cancer. Nature *469*, 314–322.

Visvader, J.E., and Lindeman, G.J. (2012). Cancer stem cells: current status and evolving complexities. Cell Stem Cell *10*, 717–728.

Vukcevic, M., Zorzato, F., Spagnoli, G., and Treves, S. (2010). Frequent calcium oscillations lead to NFAT activation in human immature dendritic cells. J. Biol. Chem. *285*, 16003–16011.

Xu, X.L., Xing, B.C., Han, H.B., Zhao, W., Hu, M.H., Xu, Z.L., Li, J.Y., Xie, Y., Gu, J., Wang, Y., and Zhang, Z.Q. (2010). The properties of tumor-initiating cells from a hepatocellular carcinoma patient's primary and recurrent tumor. Carcinogenesis *31*, 167–174.

Yamashita, T., Ji, J., Budhu, A., Forgues, M., Yang, W., Wang, H.Y., Jia, H., Ye, Q., Qin, L.X., Wauthier, E., et al. (2009). EpCAM-positive hepatocellular carcinoma cells are tumor-initiating cells with stem/progenitor cell features. Gastroenterology *136*, 1012–1024.

Yovchev, M.I., Grozdanov, P.N., Joseph, B., Gupta, S., and Dabeva, M.D. (2007). Novel hepatic progenitor cell surface markers in the adult rat liver. Hepatology *45*, 139–149.

Zhang, M., Atkinson, R.L., and Rosen, J.M. (2010). Selective targeting of radiation-resistant tumor-initiating cells. Proc. Natl. Acad. Sci. USA *107*, 3522–3527.